CORA Cork Open Research Archive
Cartlann Taighde Oscailte Chorcaí

Title	A vertical lamellae arrangement of sub-16 nm pitch (domain spacing) in a microphase separated PS-b-PEO thin film by salt addition
Author(s)	Ghoshal, Tandra; Ntaras, Christos; Shaw, Matthew T.; Holmes, Justin D.; Avgeropoulos, Apostolos; Morris, Michael A.
Publication date	2015-06-18
Original citation	Ghoshal, T., Ntaras, C., Shaw, M. T., Holmes, J. D., Avgeropoulos, A. and Morris, M. A. (2015) 'A vertical lamellae arrangement of sub-16 nm pitch (domain spacing) in a microphase separated PS-b-PEO thin film by salt addition', Journal of Materials Chemistry C, 3(27), pp. 7216-7227. doi: 10.1039/c5tc00485c
Type of publication	Article (peer-reviewed)
Link to publisher's version	http://pubs.rsc.org/en/Content/ArticleLanding/2015/TC/C5TC00485C http://dx.doi.org/10.1039/c5tc00485c Access to the full text of the published version may require a subscription.
Rights	**© The Royal Society of Chemistry 2015**
Item downloaded from	http://hdl.handle.net/10468/6778

Downloaded on 2018-09-21T13:43:13Z

UCC
University College Cork, Ireland
Coláiste na hOllscoile Corcaigh

A vertical lamellae arrangement of Sub-16 nm pitch (domain spacing) in a microphase separated PS-b-PEO thin film by salt addition

Tandra Ghoshal,[1,2*] Christos Ntaras,[3] Matthew. T. Shaw,[4] Justin D. Holmes,[1,2] Apostolos Avgeropoulos,[3] Michael A. Morris[1,2*]

[1]Materials research group, Department of Chemistry and Tyndall National Institute, University College Cork, Cork, Ireland

[2]AMBER (Advanced Materials and Biological Engineering Research Centre), Trinity College Dublin, Dublin, Ireland

[3]Department of Materials Science Engineering, University of Ioannina, Ioannina, Greece

[4]Intel Ireland Ltd., Collinstown Industrial Estate, Co. Kildare, Ireland

[*] Corresponding Author: Prof. Michael A. Morris

Tel: + 353 21 490 2180

Fax: +353 21 427 4097

E-mail: m.morris@ucc.ie

*Dr. Tandra Ghoshal

Tel: + 353 21 490 2911

Fax: +353 21 427 4097

E-mail: g_tandra@yahoo.co.in

Ultra-small feature size (~8 nm domain width) nanopatterns have been achieved using a symmetric polystyrene-b-polyethylene oxide (PS-b-PEO) block copolymer (BCP) of low molecular weight (PS and PEO blocks of 5.5 and 5.3 kg mol^{-1} respectively). The work represents the smallest feature size attained and the first observation of a well-controlled film of a perpendicularly oriented lamellar pattern in thin film form for this system. The polymer synthesized and described herein has a value χN (= 7.7), below the expected BCP phase segregation limit of 10.5. These patterns were achieved by amplification of the effective interaction parameter (χ_{eff}) of the BCP system by the addition of lithium chloride (LiCl) salt. A model where the Li^+ ions strongly coordinate with the PEO block without affecting the PS chain is proposed to explain the ordered self-assembly. The morphological and structural evolution for these PS-b-PEO/LiCl thin films was investigated by variation of the experimental parameters such as temperature, annealing time, salt concentrations, solution aging time, annealing solvent etc. All the experimental parameters have significant effects on the morphology, domain spacing, defectivity or surface roughness of these symmetric BCP thin films as evident from different microscopic and spectroscopic techniques. Possible hard mask applications in the area of lithography are demonstrated.

Introduction

The continual reduction of critical dimensions (CDs) of advanced semiconductor devices has necessitated the development of expensive multiple patterning techniques in ultraviolet (UV) lithography.[1] As an alternative, directed self-assembly (DSA) lithography is being explored as a cost-effective, robust and scalable method for next generation hole[2] and line/space patterns[3]. The most promising and advanced of the DSA techniques is the microphase separation of block copolymers (BCPs) which form a number of highly regular nanostructured morphologies due to chemical incompatibility of the blocks and depends on molecular weight, the strength of the interaction between the blocks (indicated by the Flory-Huggins interaction parameter χ), the degree of polymerization N and the volume fraction of the blocks.[4-7] For creation of line patterns, symmetric, lamellar-forming BCP systems that can exhibit domain orientation perpendicular to the substrate are of particular interest since their pattern transfer to a substrate is conceptually simple and various structures or components of integrated circuits (ICs), (e.g. contacts, interconnects, gates for the current planar as well as future 3D devices) might be fabricated.[8] Among different BCPs investigated, polystyrene-*b*-polymethylmethacrylate (PS-*b*-PMMA) has been the pre-eminent system of interest because of its availability, ease of synthesis, and established utility.[2, 9-10] However, despite considerable progress, there are challenges such as long processing times[11], and the requirement of careful interface engineering to define domain orientation[12]. Though the microphase separation can now be achieved within a short time by advanced annealing processes[13-16] the minimum feature size that can be attained is above expected roadmap targets[17].

Thus, there is a need to find alternatives to the established PS-b-PMMA system that form well-defined lamellae arrangements and are also capable of extension to sub 10 nm feature size. The polystyrene-b-polyethylene oxide (PS-b-PEO) system is an attractive alternative to PS-b-PMMA and the asymmetric, cylinder forming compositions have been well researched and

exhibits high degrees of lateral ordering within short processing times without any substrate surface modification.[18-22] Importantly, the high affinity of the ethyleneoxy segments for various cations allows this system to be used as templates for inorganic pattern development in various lithographic and biological applications[23-26]. However, lamellar forming systems are much less well researched and application in nanolithography has not been demonstrated.

Herein, we report, microphase separated perpendicularly oriented lamellae of a symmetric short chain length PS-b-PEO thin film by solvent annealing approach to achieve sub-20 nm pitch patterns. During a typical solvent annealing process, BCP thin films are exposed to solvent vapour that permeates and swells the polymer domains in order to achieve phase separation through the increased mobility of the polymer chains by plasticization effect (effectively reducing T_g)[27] and reduction of the effective interaction parameter (χ_{eff}) through dilution of the polymer chains[28]. Different solvent annealing conditions such as the rate at which the solvent is removed, the extent of swelling, the choice of solvents, and other process parameters can therefore be expected to affect the self-assembled lamellar morphology in thin films for generating networks with subtle differences in defect structure, defect density, and continuity.[29-32]

An ideal symmetric BCP (volume fraction $f = 0.5$) forms a lamellar microdomain structure when the segregation strength χN is larger than 10.5, but is disordered for smaller χN.[33] The estimated value of χN for the short chain length (5.5 kg mol^{-1} -5.3 kg mol^{-1} in this report) PS-b-PEO system is 7.71, suggesting well-defined microphase separated nanopatterns should not form after solvent annealing. The most effective way to increase the value of χ_{eff} is the addition of lithium salt into the BCP which have significant effects on the order-order and order-disorder transitions in the system[34] and shown to increase the immicibility of the two blocks with salt concentration via:[35-36]

$$\chi_{eff} = \chi + mr \qquad \text{(eq. 1)}$$

where r is the molar ratio of Li^+ ions to EO monomers and m, a parameter dependent on the anion type. Since the binding energy between Li^+ and oxygen is very large,[37] Li^+ ions are predominantly distributed within the PEO chains without affecting the PS chains. Based on the previous studies[34, 38-39] it was hoped to achieve microphase separated ordered perpendicularly oriented lamellae for the symmetric PS-b-PEO system. Morphological and structural variations were examined for different salt concentrations within the BCP and using various annealing processing parameters. We believe this is the first report of the microphase separated ordered lamellar phases of an ultra-small domain size PS-b-PEO system by the Li^+ salt addition. We demonstrate that these could create ultra small, high density, good quality Si nanopatterns which have potential in nanotechnogical applications using similar techniques to our established protocol[19, 25, 40] for the hexagonal phase PS-PEO system.

Experimental Section

Materials

Ethylene oxide (all materials Sigma Aldrich unless stated) was dried over CaH_2, purified through n-BuLi twice for 30 min at -10^0C and was then distilled into an appropriately calibrated Pyrex ampule for use. Phosphazene base (P_4-t-Bu) (1M solution in hexane), sec-BuLi (1.4 M solution in cyclohexane) and acetic acid (Panreac) were used without further purification. Benzene (Chem Lab, 99.7%) was freshly distilled from CaH_2 and polystyryl lithium ($PS^{(+)}Li^{(-)}$) and kept for further use. Styrene and dibutylmagnesium were purified through CaH_2 distillation and added to calibrated Pyrex ampules. Various other solvents/salts were used as detailed toluene, Tetrahydrofuran (THF), anhydrous alcohol (ETH), Dimethylformamide (DMF) and Lithium chloride. Single crystal (100) boron doped (P type) silicon wafers with a native silica layer were used as general substrates. Different hard mask substrates such as Si-ARC (anti-reflective coating), alumina and carbon hard mask (CHM) etc. are selected to check

the applicability of the pattern formation. For filtration, Fluoropore™ PTFE filter membranes with a pore size 0.2 μm, diameter of 25 mm thickness was used.

Polymerization

Styrene (2.5 g, 0.024 mol) was introduced from the Pyrex ampoule into a flask under high vacuum containing 200 mL of freshly distilled benzene. Approximately, 1 mmol of sec-BuLi (initiator) was added and the mixture was left to react for 24 hours at room temperature. Then, 2.5 g (0.057 mol) ethylene oxide was introduced in the mixture from a Pyrex ampule. The red solution due to active $PS^{(-)}Li^{(+)}$ became transparent after the addition of ethylene oxide. The reaction mixture was stirred for 2 h, followed by the addition of 0.80 mmol of P_4-t-Bu in order to improve the propagation reaction for the polymerization of ethylene oxide. The reaction mixture was stirred for 10 days at 40ºC. It should be noted that in this approach we used benzene as solvent rather than tetrahydrofuran as it led to stricter control of the EO polymerization reaction presumably due to its' non-polar nature. The reaction was terminated with approximately 0.50 mL of acetic acid. In Scheme 1 represents the reactions for the synthesis of the diblock copolymer.

Procedure for microphase separation

Substrates were cleaned by ultrasonication in acetone (30 min) and toluene (30 min) and dried under nitrogen. A 1 wt% PS-*b*-PEO solution in toluene (5 gm) was stirred for 12 h at room temperature. LiCl was dissolved in ethanol and in THF separately to make 2.5 mg/mL solution. Then the necessary amount of LiCl/ethanol or LiCl/THF solution (varying from 0.025 ml to 2 ml) was added to the prepared PS-*b*-PEO/toluene solution with a micropipette. The solution was again stirred for different times between 15 min to 2h for salt complexation to take place. The resultant solution was filtered and spin coated immediately onto the substrate at 3000 rpm for 30 s. The films were exposed to toluene/THF/DMF vapour placed at the bottom of a closed vessel kept at different temperature ranging from 40^0 C-70^0 C for different time period (15 min

to 2 h) to induce microphase separation. After solvent annealing for the desired time, the films were dried under nitrogen.

Characterizations

GPC measurements were carried out with THF as eluent, using the PL GPC-50 (Polymer Laboratories) instrument at 40ºC while the average molecular weight was determined with membrane osmometry using Osmomat 090 (Gonotec). ^{1}H-NMR experiments were performed in $CDCI_3$, on a Bruker AVANCE II spectrometer at 250 MHz. Surface morphologies were imaged by scanning probe microscopy (SPM, Park systems, XE-100) in tapping mode and Helium ion scanning electron microscopy (Carl Zeiss HIM). The film thicknesses were measured by optical ellipsometer (Woolam M2000) and electron microscopy (i.e. cross-sections). Sample cross-sections were prepared for the Transmission electron microscopy (TEM) cross sectional imaging using an FEI Helios Nanolab 600i system containing a high resolution Elstar™ Schottky field-emission SEM and a Sidewinder FIB column. These were then imaged by transmission electron microscopy (TEM, JEOL 2100 and TEM, FEI Titan). Fourier Transform Infrared Spectrometry (FTIR) spectra were recorded on infrared spectrometer (IR 660, Varian).

Results and Discussion

Characterizations of the synthesized block copolymer

The characterization results for the synthesized BCP are given in Table 1 reveal lamellar phase system with the molecular weight of the blocks of PS = 5.5 and PEO =5.3 kg mol^{-1}. In Scheme 2a, the final GPC chromatograph is shown, indicating the very low polydispersity of the final diblock copolymer. ^{1}H-NMR spectra (Scheme 2b) indicates shifts corresponding to δ = 4.40 - 5.00 (CH,O) for poly(ethylene oxide) segments and 6.80 - 7.50 (aromatic, C-H) for polystyrene respectively. The fact that the molecular characteristics from GPC and ^{1}H-NMR for the weight fraction are almost identical indicates molecular and compositional homogeneity.

Microphase separation of PS-PEO thin film with LiCl-ethanol and LiCl-THF solution

In order to achieve a microphase separated ordered perpendicularly oriented lamellae structure of the PS-PEO thin film, different solvent and thermal annealing approaches (films exposed to different solvents at different temperature and time) were applied. As might be expected, in the absence of the lithium salt, there is no indication of the formation of ordered surface structures for any conditions used suggesting no microphase separation occurred or that the arrangement of the lamellae was parallel to the substrate because of preferential PEO-substrate interactions at both terminating interfaces[18] (See Supporting Information, Figs. S1 and S2). The morphology of the PS-b-PEO thin film following solvent annealing in toluene at 60^{o} C for 30 min with the addition of 0.05 ml of LiCl-ethanol and LiCl-THF are shown in Fig. 1. As-cast films possess a disordered morphology without any indication of feature periodicity. Solvent annealing results in the formation of perpendicularly oriented ordered arrangement of adjacent PS and PEO lamellae (PEO is darker in colour in the AFM image). Note that thermal annealing at the same temperature in the absence of the solvent has no effect on the as-cast disordered structure demonstrating that toluene is a necessary component to induce phase separation. The films prepared with LiCl-THF (Figs. 1c and d) exhibits smoother surface area and of uniform thickness across the substrate area compared to the LiCl-ethanol (Figs. 1a and b) systems. More micro-defects in the form of small particulate (diameter 25-250 nm) or homogeneously distributed dark spots without any patterns are observed for the LiCl-ethanol systems for all the solvent annealed films. Although local area defects are observed for the LiCl-THF system, no large area dewetting or thickness undulation is evident. Further, longer line-like morphology is noticed. The measured average lamellar domain spacing that follow a single definite in-plane orientation is 15 nm (AFM and SEM measurements) and this value (+/- 2%) was observed for all films which remained identical for the films prepared from both LiCl-THF and LiCl-ethanol. These data suggest that microphase separation is the direct result of Li^{+} insertion

within BCP (PEO block). The film thickness was measured at different areas of the film surface by ellipsometry with an average value of ~ 22 nm ± 2 nm. The average water contact angle of the film before and after solvent annealing are 94 ^{0} and 53^{0} respectively. This indicates that the film surface is hydrophobic and PS rich before annealing which changed to 53^{0} for the solvent annealed perpendicularly oriented ordered lamellar structure. The contact angle varied between 53^{0}-57^{0} might be due to the thickness variation.[41] Note that no surface treatment or modifications with random copolymer brushes is necessary to ordain the vertical domain orientation.

Morphology and interfaces by cross sectional TEM

The internal morphology and interface of the film with the substrate surface is further analysed through the cross-sectional FIB thinned TEM. Generally, the similarity of the PS (1.05 g cm^{-3}) and PEO (1.12 g cm^{-3}) densities results in featureless TEM micrographs[24] and this was observed here. However, the PEO selective inclusion of Li^{+} ions should result in an enhancement of the electron contrast. Fig. 2 shows the cross-sectional TEM image of the periodic ordered lamellar film prepared with the addition of LiCl-THF after solvent annealing in toluene at 60^{o} C for 30 min. The image did not reveal the lamellar structure but instead periodic dark spots of varying diameter of 2-6 nm in the centre of the film. The regions are not spanning over the entire thickness of the film and also the diameter is not consistent with either PS or PEO microdomain dimensions. The elliptical areas within the film can be seen at a similar repeat distance of 15 nm (Fig. 2b) as the lamellar spacing observed before (Fig. 1) suggests the included Li^{+} ions segregate into the centre of the PEO domains. In this way, the inclusion of the ions does not allow the lamellae arrangement throughout the entire film thickness to be revealed. The polymer film shows no indication of deformation or delamination at the substrate interface and the TEM derived thickness of 22 nm is consistent with ellipsometry measurement.

The arrangement of the lamellae was revealed by the 'inorganic inclusion' technique adopted by us before.[18-19, 24] In this technique, a metal precursor-alcohol solution, nickel nitrate hexahydrate ($Ni(NO_3)_3,6H_2O$) in this case, was spin coated onto the microphase separated thin film. The hydrophobic nature of PS limits metal ion inclusion into the PS lamellae whilst selective inclusion into the BCP template is favoured by the affinity of PEO with the ionic solution. The spin coating procedure is highly efficient and it is suggested that PEO accelerates the metal ion inclusion process probably via either intra- or intermolecular coordination via electron donation from the PEO block to oxygen species in the alcohol molecule. Thus, the selective inclusion of the inorganic molecule into the PEO lamellae enhances the electron contrast. The cross-sectional TEM image in Fig. 2c shows the ordered arrangement of the PEO lamellae with the inorganic inclusion without removing the polymer. This confirms the perpendicular, equally spaced, ordered arrangement of the PS and PEO lamellae with a spacing of ~ 15 nm. Further, significant contrast enhancement is noticed which shows the PEO lamellae span over the entire thickness of the film. A very thin (~ 2 nm) silica layer exists on top of the Si substrate. Note that the concentration of the inorganic precursor was optimized in order to avoid the overfilling of the PEO lamellae.

Compositional analysis by FTIR

FTIR spectroscopy was used here to provide information regarding the lithium ion-polymer interactions and the presence of residual or trapped solvent in the microphase separated nanostructured thin films. Fig. 3 shows representative FTIR spectra of the BCP thin films for the addition of LiCl-THF and LiCl-ethanol after solvent annealing in toluene at 60^o C for 30 min. All the spectra recorded display features typical of the PS and PEO blocks. Peaks around 738 cm^{-1} (benzene bending), 1620 cm^{-1}, and 1452 cm^{-1} (benzene ring stretching), weak overtone and combination bands in the range of 1655-2000 cm^{-1} can all be attributed to polystyrene.[42] No shift or noticeable intensity change for both the systems was observed for

the polystyrene peaks confirm that the lithium salt does not interact with the PS microdomain. However, small shifts or combination of the peaks was observed for the PEO blocks. The ion dipole interaction between Li^+ ions and the C-O-C group of PEO imposes appreciable effects on the fundamental characteristic peaks at 825 cm^{-1} ($\rho(CH_2)$ + δ(C-O-C)) , 945 cm^{-1} ($\rho_s(CH_2)$ + ν(C-C)), 960 cm^{-1} ($\rho_{as}(CH_2)$ + $\nu(CH_2)$), 1060 cm^{-1} (ν(C-C) + $\rho(CH_2)$), a triplet 1145, 1093, 1060 cm^{-1} (ν_s(C-O-C)), 1241cm^{-1} ($\tau_s(CH_2)$), 1279 cm^{-1} ($\tau_{as}(CH_2)$), 1456 cm^{-1} ($\delta_s(CH_2)$), 1466 cm^{-1} ($\delta_{as}(CH_2)$), 2881 cm^{-1} ($\nu_s(CH_2)$), and 2946 cm^{-1} ($\nu_{as}(CH_2)$) of PEO block[43] where the symbols corresponds to ν = stretch, ν_{as}= asymmetrical stretch, ν_s = symmetrical stretch, δ = deformation mode, ρ = rock, τ = twist. The peak at 825 cm^{-1} splits into two, a weak peak at 819 cm^{-1} and a broad band at 886 cm^{-1}, integration of the peak at 955 cm^{-1} implies the change in environment surrounding PEO due to Li^+ ions. The disappearance of the peak at 1060 cm^{-1} and the existence of one sharper and stronger peak at 1109 cm^{-1} indicating coordination of Li^+ ions with PEO. The shifting of the bending modes of PEO to 1245, 1295 cm^{-1} caused by the shifting in the electron surrounding of the carbon backbone as a result of the coordination of Li^+ ions and the oxygen atoms of the C–O–C group.[43] The $\delta_s(CH_2)$ and $\delta_{as}(CH_2)$ at 1456 and 1466 cm^{-1} respectively, merge into a strong peak with increased intensity centred at 1452 cm^{-1}. Similar peak shift observed for the peaks at 2855 and 2927 cm^{-1}. The appearance of two weak peaks at 1310 and 1375 cm^{-1} corresponds to the crystalline phase of PEO related to the transition dipole moment orientated parallel and perpendicular to the PEO chain axis, respectively.[44] This suggest that some sort of crystallization of PEO occurred due to solvent annealing of the films at a temperature higher than the melting point of PEO, but most of the fractions remained in the amorphous phase as evident from the TEM data. No residual or trapped solvent (Toluene/THF) was detected in the spectra within the BCP films. Further, the band due to the OH stretching vibration between 3100-3600 cm^{-1} is also not evident. But small and FTIR indictable amounts of trapped or residual solvent are probably present inside the film since

when the microphase separated film was rapidly removed from the solvent vapour environment, there is always certain amount of solvent trapped inside the film which cannot evaporate at room temperature despite the low boiling point of toluene. This data suggests the interaction between the ether oxygen of PEO and the Li^+ ion is dominant while the PS domain remained relatively unaffected.

Effects of solvent annealing temperature and time

As outlined above, morphological changes of the PS-b-PEO/LiCl system with annealing temperature (varied from 40^o C to 70^o C) and time (15 min to 2h) were studied. Data are summarized in Fig. 4. As evident from the AFM image in Fig. 4a, the phase separation begins at a temperature of 40^o C for 30 min, but no ordered structure is observed. Further data emphasizes disordered and deformation of the film (See Supporting Information). A reasonably well ordered perpendicularly oriented fingerprint morphology is realized for the film solvent annealed at a temperature of 50^o C for 30 min (Fig. 4b). The measured average lamellar domain spacing is 15 nm and the ellipsometry measured thickness of the film is 22 ± 2 nm. However, film self assembled at 60^o C (Figs. 4c-h) have lower defect density with the branch and end point densities being noticeably lower at the higher temperature. Lamellae arrangements formed by BCP systems during solvent annealing have low defect densities that are generally correlated to a decrease in the average interfacial curvature between domains. The persistence length of domains observed at 60 °C is 2-3 times than that seen at 50 °C. It is not the case that lower defect densities must necessarily lead to lamellae with long persistence lengths; network topologies with high tortuous pathways (lamellae) between network nodes (defect such as branches) can be envisioned for any node density. However, there is a clear correlation between defect density and persistence length in lamellar BCP thin films. This is probably a result of the defect annihilation process that allows high energy defects (such as

disclinations/dislocations) to be removed whilst simultaneously reducing the block-block interfacial area which contribute less to the total energy of the system.

Increasing solvent annealing time also leads to defect annihilation in the microphase separated BCP thin films, and therefore, it is significant to study the morphological change with time. Figs. 4c-h displays the AFM and SEM images showing the progressive change in the domain morphologies with solvent annealing time at a temperature of 60^{o} C. Small persistence length fingerprint patterns is observed after 15 min annealing time (Figs. 4c and d). As well as obvious pattern defects, many film defects and height variation are observed. Junctions, bends and interconnects are frequent but the surface of the films clearly indicates microphase separation after 15 min solvent exposure. As above, 30 min solvent exposure results in a well-defined polymer arrangement (Fig. 1c and d). Annealing for 45 minutes increases in increased persistence length and AFM images shown in Fig. 4e indicate a well-ordered system. However, SEM data in Fig. 4f show the film to be more defective than the corresponding AFM and, in particular, it can be seen that lamellae can be connected through the sidewalls. Annealing for 1 h results in considerable pattern degradation (Figs. 4g and h). Large areas of domain agglomeration are seen as wide bands are formed. It is suggested these are due to local reorientation into a parallel (to the surface plane) arrangement. There is also loss of order and higher defect densities. No significant variation in the domain spacing (~ 15 nm) or the film thicknesses over the time period studied is observed.

Effects of salt concentration and solution aging time

A linear relationship has been reported between χ_{eff} and the salt concentration in the cylinder forming PS-b-PEO : LiX (X = anions) system.[35] For the lamellar phase we have determined the minimum amount of salt required for the desired single phase lamellar pattern without any pattern degradation or any secondary patterns formed on the film surface. Figs. 5a-d shows the surface morphology and topography of the films for different salt concentration where the LiCl-

THF solution is stirred for 30 min. Microphase separated perpendicularly oriented ordered lamellae is observed for all the concentrations varying from 0.05 ml to 1.5 ml across the whole substrate whereas an increment in the defect density is observed. However, at volume additions of 0.025 ml and less, no microphase separation of the film is observed. With increasing the LiCl-THF content to 0.05 ml, well resolved periodic ordered structure are formed all over the substrate surface. At lower concentrations (< 1 ml), few features indicative of inorganic materials are observed suggests that the lithium ions are well dispersed and distributed uniformly throughout the PEO domains. However, elongated regions suggestive of aggregation are seen in a few parts of the film. Secondary overlayers are formed in few parts of the film surface with increasing the LiCl-THF content to 1 ml (Fig. 5a) and the frequency of these defects increases with increasing the LiCl-THF content to 1.25 ml (Figs. 5b and c) and 1.5 ml (Fig. 5d). But the ordered lamellar morphology maintained in the remaining parts of the film surface. It is suggested that these are thin layers of lithium hydroxide at the surface. At concentrations of 2 ml and above (data not shown), distinct 3D particulates (of LiOH presumably) are observed. The domain spacing is found to slightly increase from 16 nm to 17 nm with increasing the salt concentration as might be expected.[45-46] The increase in the domain spacing can be attributed to the effective increase in the interaction parameter results in the chain stretching caused by the coordination of ions with the polymer chain as well as the additional volume of the added salt.[35, 47-48]

The aging (stirring time) of the polymer-LiCl solution also has significant morphological effects. The minimum stirring period required in order achieving an ordered lamellar structure and a smooth film surface is determined. 30 min is the minimum stirring time to attain ordered microphase separated structures across the substrate and below this only isolated regions of order are observed. Increasing the stirring time to 45 min (Fig. 5e) and 1h (Fig. 5f), the film maintains the long range ordered lamellar structures but the defect frequency (in the form of

these discrete linear regions or particulates) increased with time. With increasing the stirring time for more than 1h, nanoparticles in the range of 20-200 nm are observed throughout the film surface (Fig. 5g) and eventually structural degradation (Fig. 5h) occurs.

These data can be explained. The LiCl is well dispersed and stable in THF and forms a colourless and transparent solution. No trace of precipitation observed with the stirring time but it is suggested that the particulates form because the solution is hygroscopic and exposure to atmospheric moisture results in the formation of nanosized lithium hydroxide (LiOH) clusters or ionic micelles within the solution. With increased aging time or concentration these become aggregated and increased in size (van der Wals forces). Eventually these become large enough to sterrically hinder and/or reduce the concentration in the PEO below the critical amount and so hinder formation of ordered arrangements. In this way, filtration is a critical component of this process if optimum, ordered arrangements are to form.

Effects of annealing solvents

The annealing solvent/s plays an important role in achieving stable lamellar morphologies with low-defect densities. We have investigated the microphase separation under toluene, THF and toluene/THF (1:1 volume ratio) mixtures. In all cases, microphase separation occurred resulting in lamellar networks all over the substrate surface. Following annealing in THF (Fig. 6a) and THF/toluene (Fig. 6b), the films are noticeably more defective with significant thickness variation and low persistence length domain structures compared to those solvent annealed in toluene in similar condition (60^{o} C for 30 min). The domain spacing remains unchanged but the THF annealed film is slightly thicker (~ 26 nm) compared to those annealed in toluene. Although PS and PEO both dissolves in toluene and THF, these solvents are selective towards PS and should behave similarly ($\delta_{Tol} - \delta_{PEO}$ = 1.9 MPa$^{1/2}$, $\delta_{THF} - \delta_{PEO}$ =1.7 MPa$^{1/2}$, $\delta_{Tol} - \delta_{PS}$ =0.3 MPa$^{1/2}$, $\delta_{THF} - \delta_{PS}$ = 0.5 MPa$^{1/2}$) Note δ_{Tol} = 18.3, δ_{PEO} = 20.2, δ_{THF} = 18.5 and δ_{PS} = 18.0 MPa$^{1/2}$.[19] It is suggested that the differences between films annealed in toluene only and THF

containing vapour is due to the lower boiling point of THF (66^{o} C) compared to toluene (111^{o} C). Thus, THF annealed films are more swollen, return to a non-swollen state quicker than equivalent toluene conditions. This will lead to a higher number of kinetic defects and this is seen in the increased film thickness due to frozen-in free volume. As the solvent is close to boiling point during annealing, condensation might also result in damage to liquid at the surface. Thus, THF is not selected as a preferred annealing solvent in this case. Generally, anhydrous high quality toluene is used for annealing favours enthalpically long, straight polymer chains extending away from the interface, reduce the entropic contribution of each chain, reducing structural transition resulting a stabilized lamellar network all over the substrate.[49]

Surface morphology on different substrate

As well as being technologically important as hard mask substrates used in lithography to define high aspect ratio features, we examined a number of different substrates to assess how an unexpected morphology of vertically orientated lamellae is formed contrary to what might be expected. This is important for possible lithographic applications and the formation of nanowire structures. In the PS-b-PMMA system, this requirement has led to the development of random polymer brush and surface functionalization techniques to define this orientation perfectly.[25] No such technique was required here despite that fact that the PS-b-PEO system has a greater χ value than PS-b-PMMA and should be more prone to a parallel orientation. This could be due to a fortuitous surface interface chemistry match (i.e. neutrality) and in order to understand this orientation a number of different substrates Si-ARC (anti-reflective coating), alumina and carbon hard mask (CHM) were investigated. The morphological evolution of the PS-b-PEO/LiCl system is examined. As shown in Fig. 7a, well resolved long range ordered perpendicularly oriented lamellar morphology is formed on top of Si-ARC substrate. No significant variation in the domain spacing or film thickness is observed. Interfacial bending

and smaller persistence length lamellar network formed compared to the Si substrate. Similar morphological features are achieved for the alumina substrate but thickness undulation and pattern degradation is noticed throughout the substrate surface (Fig. 7b). In comparison, CHM substrate gives longer persistence length long range ordered lamellae with smooth and uniform film surface (Fig. 7c). The wettability, surface composition and roughness might play important role in determining the morphological behaviour. These have very different surface chemistries as indicated by contact angles of for the Si-ARC, alumina and CHM substrates are 31^0, 76^0 and 38^0 respectively. The polymer solution wet the substrate surface more uniformly due to better wettability of the Si-ARC and CHM substrates compared to alumina results a uniform film over the substrate area. These data on the different substrates suggest that the vertical morphology is not defined by surface chemistry. These results are considered further below.

Discussion

In this report, a low molecular weight PS-b-PEO BCP was shown to form well-ordered lamellar structures despite a sub-optimum value of $\chi N = 7.71$. However, the segregation strength (χN) has been increased by the addition of ions in micromolar or millimolar concentrations as reported by Zhang et al. which can change the morphology of "crew-cut" aggregates of amphiphilic BCP in dilute solutions.[50] It was also demonstrated that the addition of small amounts of alkali halide or metal salts (of the order of a few ions per chain) into the cylindrical phase PS-PEO system, where the salts coordinates with the PEO block, showed long range positional correlations of the microdomains in the swollen state.[22] In the same way, the order-disorder transition temperature (T_{ODT}) can be increased by tens of degrees by salt addition.[51] In simple terms there is an enhancement of the χ_{eff} with the formation of lithium-PEO complexes.[52-53] Generally, the attractive force between the cation and the crown ethers is known to be purely electrostatic (ion-dipole interactions) giving strongly bonded complexes.[39] The strong binding will clearly affect the thermodynamics, solvation energy of the anions and

miscibility of the system.[34] It has been proposed that the oxygen atoms belonging to the PEO chain coordinate the cations and localized in the middle of the PEO lamellae in the form of pseudo ionic micelles due to nonuniform local stresses in the lamellae and the coupling between Li^+ coordination and these stresses.[38-39] This work provides clear and direct evidence of this proposal as evidenced by TEM cross-sections which snapshot this phenomena. These coordinated lithium ions creates a separation of charge (cation-anion) which leads to periodically ordered self-assembled structures on the surface. This ion-containing binary BCP system can be described with a new χ_{eff} as

$$\chi\text{eff}\,(\text{r}) = \frac{A(r)}{T} + B(r) \qquad \text{(eq. 2)}$$

where r is as defined above and in this work is calculated as ~ 0.025. As reported by Wanakule et al. that the value of m in equation (1) is a system dependent constant and found to vary with anion radius (1.81 Å in this case).[36, 54] The value of m in the case of Li ClO_4 in PS-PEO is 5.53 at 166° C.[38] Taking this into account, the calculated value of χ_{eff} is 20.8. Experimentally, χ_{eff} can be estimated from the change in structure factor of the disordered phase, the shift in the phase boundaries and the change in domain spacing of the ordered phase[38] as well as salt concentration, temperature, salt counter ions and chain conformation.

For a BCP thin film, the surface/interface energies as well as the interplay between the film thickness and the natural period plays important role in the phase behaviour of BCP.[12, 55] For most of the symmetric BCP system studied to date, careful manipulation of the interfacial energies is needed to achieve the monolayer of perpendicular orientation of the lamellae.[56-58] For the PS-b-PEO system, the blocks exhibit asymmetric affinities for the solid substrate and the air interface where the hydrophilic PEO will preferentially wet the substrate surface (favourable PEO-substrate interactions) whilst PS will tend to segregate to a vacuum interface to form a PS-rich layer (PS has a lower surface energy, γ_{PS} = 33 mNm^{-1}; γ_{PEO} = 43 mNm^{-1}).[18] One can also suggest the solubility parameter differences (see above) would favour the

formation of a PS wetting layer at the polymer-solvent interface during solvent annealing. Thus, an adjacent layer of PS and PEO parallel to the substrate surface is expected after microphase separation. This is illustrated in Scheme 3a. It may be concluded that the insertion of Li is strongly affecting the film orientation since a vertical orientation is observed (Scheme 3b).

Wang et al.[59-60] proposed that adding LiCl salt into PS-b-PMMA copolymer films can direct the orientation of the lamellar microdomains by modification of polymer groups that interact strongly with the ion and the surface. These are simple and attractive models but we believe the explanations for behaviour are more nuanced. It is clear that addition of polar entities to a BCP can enhance χ (as clearly demonstrated here) but the mechanism is largely unproven since the location of the added ions is generally unknown. However, the TEM data provides evidence that the lithium ions are located in the centre of the PEO block (coordinated via the electron pair on the oxygen). This suggests that the lithium ions are less favourably located at either the film-substrate, film-air or PS-b-PEO interfaces. This probably results from the high energy interactions of the highly polar ions and the non-polar PS block and the thermodynamic improbability of forming charged surfaces. We note that it must be highly thermodynamically favourable that the lithium ions located within the centre of the PEO regions only because no domain contrast is seen in either SEM or TEM on lithium addition. Note that locations within the centre of the blocks is also favourable because it maximizes the distance and minimizes the interactions between the Li^+-Li^+ centres. Assuming this model to be correct, we can directly compare the two possible orientations described in Scheme 3. It can instantly be seen that the vertical orientation maximizes the distance of the lithium centres from the interfaces and maximizes the distance between these centres and so lowers the energy of the system considerably. We suggest that this is a possible explanation for this vertical alignment in all samples observed here across a range of substrates.

We should also comment that these surfaces are only metastable and on extended ambient exposure, the lithium will tend to segregate due to hydrolysis and carbonations via the reactions:

$Li^+ + H_2O$ --------- $LiOH + H^+$

$2Li^+ + CO_2 + O^{2-}$ ---------- Li_2CO_3

This leads to segregation of the compounds to the surface and growth of particulates.

The other issue that must be addressed is the role of lithium in enabling this ultra-small scale self-assembly with particular reference to the fabrication of semiconductor devices. This is through a pattern transfer process into the Si substrate. Diffusion of lithium into the silicon would have a significant deleterious effect on device performance. At room temperature, crystalline Si goes through a single crystalline-to-amorphous phase transformation during the first lithiation and remains amorphous afterwards[61] and thus both chemical and physical robustness of the devices is an issue. However, despite exhaustive analysis, no evidence for lithium at the surface of these materials was found after thermal treatments or UV/ozone treatments to remove the polymer. This may be because of the relatively small amounts present. Assuming the total volume of PEO lamellae are swollen by around 20% by the solvents used in the coating solution (Toluene and THF) (and since this is spun-on this is probably overestimated) than the surface concentration must be less than 10^{14} atoms cm^{-2}. We would also suggest that the oxidative treatments used to remove polymer could result in the volatilization of lithium through carbonyls etc. The other important consideration is that there is a well-defined silicon oxide layer between the lithium and the silicon. Lithium and silica form a series of silicates and silica acts as a barrier for diffusion of lithium ions to the substrate.[62] Thus, through a pattern transfer process, the lithium present should be either removed in the etch or passive oxide removal steps. Thus, it is suggested that this may not be

a significant problem but we will be carrying out studies of pattern transferred structures to assess the effects quantitatively in future work.

Conclusions

In summary, we have achieved microphase separated well-ordered perpendicularly oriented lamellae for a symmetric PS-b-PEO system with a domain spacing of ~16 nm by a simple solvent annealing process with a χN value below the BCP phase segregation limit. By enabling tight complexation between Li^+ ion and the PEO block through salt (LiCl) addition, enhances the χ_{eff} of the BCP system with low Molecular weights and triggered a disorder-to-order-transition to obtain the phase separation. Though the mechanism for effective increase of χ is complex and depends on the localization of the ions within the centre of the PEO blocks. Vertical orientation of the lamellar structure is favourable and appears not to be dependent on modification of the block – substrate interactions but rather on the interactions of the polar groups with the interfaces. The minimum amount of salt and the time required for the PEO-ion coordination is investigated through the morphological and structural observation of the thin films for different salt concentrations and aging time of the BCP-salt systems. The long range ordered self assembly is obtained at a lower temperature range (50-60^o C) annealed for 30 min without the need of any surface modifications. THF proved to be a good solvent for the solvation of Li salt into the BCP system instead of ethanol whereas toluene is a selective annealing solvent realizing low defectivity nanofeatures. The materials and processes are robust. It is applicable to a wide range of substrates and occurs over a wide range of solvent annealing conditions. The ease with which these very small features can be formed might be applicable for developing ultra-small devices via techniques such as pattern transfer.

AUTHOR INFORMATION

Corresponding Authors

*Email: m.morris@ucc.ie; g_tandra@yahoo.co.in

Notes

The authors declare no competing financial interest.

Acknowledgements

We acknowledge financial support from the Science Foundation Ireland AMBER grant 12/RC/2278 and Semiconductor Research Corporation (SRC) grant 2013-OJ-2444. The contribution of the Foundation's Principal Investigator support is also acknowledged.

Notes and references

1 Emerging Research Devices. In *The International Technology Roadmap for Semiconductors*, 2011; pp 1-77.

2 R. Ruiz, H. M. Kang, F. A. Detcheverry, E. Dobisz, D. S. Kercher, T. R. Albrecht, J. J. de Pablo and P. F. Nealey, *Science,* 2008, **321**, 936-939.

3 J. Y. Cheng, D. P. Sanders, H. D. Truong, S. Harrer, A. Friz, S. Holmes, M. Colburn and W. D. Hinsberg, *ACS Nano,* 2010, **4**, 4815-4823.

4 D. Borah, M. Ozmen, S. Rasappa, M. T. Shaw, J. D. Holmes and M. A. Morris, *Langmuir,* 2013, **29**, 2809-2820.

5 Q. Wang, P. F. Nealey and J. J. de Pablo, *Macromolecules,* 2001, **34**, 3458-3470.

6 S. Rasappa, D. Borah, C. C. Faulkner, T. Lutz, M. T. Shaw, J. D. Holmes and M. A. Morris, *Nanotechnology,* 2013, **24**.

7 D. Borah, M. T. Shaw, S. Rasappa, R. A. Farrell, C. O'Mahony, C. M. Faulkner, M. Bosea, P. Gleeson, J. D. Holmes and M. A. Morris, *J. Phys. D-Appl. Phys.,* 2011, **44**, 174012.

8 J. Xu, S. W. Hong, W. Y. Gu, K. Y. Lee, D. S. Kuo, S. G. Xiao and T. P. Russell, *Adv. Mater.,* 2011, **23**, 5755-5761.

9 C. M. Bates, T. Seshimo, M. J. Maher, W. J. Durand, J. D. Cushen, L. M. Dean, G. Blachut, C. J. Ellison and C. G. Willson, *Science,* 2012, **338**, 775-779.

10 K. Galatsis, K. L. Wang, M. Ozkan, C. S. Ozkan, Y. Huang, J. P. Chang, H. G. Monbouquette, Y. Chen, P. Nealey and Y. Botros, *Adv. Mater.,* 2010, **22**, 769-778.

11 D. J. C. Herr, *J. Mater. Res.,* 2011, **26**, 122-139.

12 P. Mansky, Y. Liu, E. Huang, T. P. Russell and C. J. Hawker, *Science,* 1997, **275**, 1458-1460.

13 C. C. Liu, C. J. Thode, P. A. R. Delgadillo, G. S. W. Craig, P. F. Nealey and R. Gronheid, *J. Vac. Sci. Technol. B,* 2011, **29**.

14 A. M. Welander, H. M. Kang, K. O. Stuen, H. H. Solak, M. Muller, J. J. de Pablo and P. F. Nealey, *Macromolecules,* 2008, **41**, 2759-2761.

15 F. Ferrarese Lupi, T. J. Giammaria, G. Seguini, M. Ceresoli, M. Perego, D. Antonioli, V. Gianotti, K. Sparnacci and M. Laus, *J. Mater. Chem. C,* 2014, **2**, 4909-4917.

16 M. Perego, F. Ferrarese Lupi, M. Ceresoli, T. J. Giammaria, G. Seguini, E. Enrico, L. Boarino, D. Antonioli, V. Gianotti, K. Sparnacci and M. Laus, *J. Mater. Chem. C,* 2014, **2**, 6655-6664.

17 Y. Zhao, E. Sivaniah and T. Hashimoto, *Macromolecules,* 2008, **41**, 9948-9951.

18 T. Ghoshal, M. T. Shaw, C. T. Bolger, J. D. Holmes and M. A. Morris, *J. Mater. Chem.,* 2012, **22**, 12083-12089.

19 T. Ghoshal, R. Senthamaraikannan, M. Shaw, P. Carolan, J. Holmes, S. Roy, M. Morris, *Scientific Reports,* 2013, **3**, 2772.

20 P. Mokarian-Tabari, T. W. Collins, J. D. Holmes and M. A. Morris, *ACS Nano,* 2011, **5**, 4617-4623.

21 J. Bang, U. Jeong, D. Y. Ryu, T. P. Russell and C. J. Hawker, *Adv. Mater.,* 2009, **21**, 4769-4792.

22 S. H. Kim, M. J. Misner, L. Yang, O. Gang, B. M. Ocko and T. P. Russell, *Macromolecules,* 2006, **39**, 8473-8479.

23 S. Kim, S. Lee, J. Ko, J. Son, M. Kim, S. Kang and J. Hong, *Nat. Nanotechnol.,* 2012, **7**, 567-571.

24 T. Ghoshal, T. Maity, J. F. Godsell, S. Roy and M. A. Morris, *Adv. Mater.,* 2012, **24**, 2390-2397.

25 T. Ghoshal, R. Senthamaraikannan, M. T. Shaw, J. D. Holmes and M. A. Morris, *Nanoscale,* 2012, **4**, 7743-7750.

26 C. L. Ren, W. D. Tian, I. Szleifer and Y. Q. Ma, *Macromolecules,* 2011, **44**, 1719-1727.

27 T. S. Chow, *Macromolecules,* 1980, **13**, 362-364.

28 E. Helfand and Y. Tagami, *J. Chem. Phys.,* 1972, **56**, 3592-&.

29 Y. Xuan, J. Peng, L. Cui, H. F. Wang, B. Y. Li and Y. C. Han, *Macromolecules,* 2004, **37**, 7301-7307.

30 R. Guo, H. Y. Huang, Y. Z. Chen, Y. M. Gong, B. Y. Du and T. B. He, *Macromolecules,* 2008, **41**, 890-900.

31 Y. S. Jung and C. A. Ross, *Adv. Mater.,* 2009, **21**, 2540-+.

32 Y. Wang, X. D. Hong, B. Q. Liu, C. Y. Ma and C. F. Zhang, *Macromolecules,* 2008, **41**, 5799-5808.

33 F. S. Bates and G. H. Fredrickson, *Phys. Today,* 1999, **52**, 32-38.

34 I. Nakamura, N. P. Balsara and Z. G. Wang, *Phys. Rev. Lett.,* 2011, **107**.

35 W. S. Young and T. H. Epps, *Macromolecules,* 2009, **42**, 2672-2678.

36 N. S. Wanakule, J. M. Virgili, A. A. Teran, Z. G. Wang and N. P. Balsara, *Macromolecules,* 2010, **43**, 8282-8289.

37 A. Eilmes and P. Kubisiak, *J. Phys. Chem. A,* 2008, **112**, 8849-8857.

38 F. F. Xue and S. C. Jiang, *RSC Adv.,* 2013, **3**, 23895-23908.

39 F. Meyer, J. M. Raquez, P. Verge, I. M. de Arenaza, B. Coto, P. Van Der Voort, E. Meaurio, B. Dervaux, J. R. Sarasua, F. Du Prez and P. Dubois, *Biomacromolecules,* 2011, **12**, 4086-4094.

40 T. Ghoshal, R. Senthamaraikannan, M. T. Shaw, J. D. Holmes and M. A. Morris, *Adv. Mater.,* 2014, **26**, 1207-1216.

41 Y. Li, J. Q. Pham, K. P. Johnston and P. F. Green, *Langmuir,* 2007, **23**, 9785-9793.

42 K. Ibrahim, A. Salminen, S. Holappa, K. Kataja, H. Lampinen, B. Lofgren, J. Laine and J. Seppala, *J. Appl. Polym. Sci.,* 2006, **102**, 4304-4313.

43 L. H. Sim, S. N. Gan, C. H. Chan and R. Yahya, *Spectroc. Acta Pt. A-Molec. Biomolec. Spectr.,* 2010, **76**, 287-292.

44 H. Tadokoro, Y. Chatani, T. Yoshihara, S. Tahara and S. Murahashi, *Makromolekulare Chemie,* 1964, **73**, 109-127.

45 J. Rosedale, F. S. Bates, K. Almdal, K. Mortensen and G. D. Wignall, *Macromolecules,* 1995, **28**, 1429-1443.

46 K. Almdal, K. Mortensen, A. J. Ryan and F. S. Bates, *Macromolecules,* 1996, **29**, 5940-5947.

47 I. Gunkel and T. Thurn-Albrecht, *Macromolecules,* 2012, **45**, 283-291.

48 A. Noro, Y. Sageshima, S. Arai and Y. Matsushita, *Macromolecules,* 2010, **43**, 5358-5364.

49 I. P. Campbell, C. L. He and M. P. Stoykovich, *ACS Macro Lett.,* 2013, **2**, 918-923.

50 L. F. Zhang, K. Yu and A. Eisenberg, *Science,* 1996, **272**, 1777-1779.

51 D. H. Lee, H. Y. Kim, J. K. Kim, J. Huh and D. Y. Ryu, *Macromolecules,* 2006, **39**, 2027-2030.

52 T. H. Epps, T. S. Bailey, H. D. Pham and F. S. Bates, *Chem. Mat.,* 2002, **14**, 1706-1714.

53 T. H. Epps, T. S. Bailey, R. Waletzko and F. S. Bates, *Macromolecules,* 2003, **36**, 2873-2881.

54 N. S. Wanakule, A. Panday, S. A. Mullin, E. Gann, A. Hexemer and N. P. Balsara, *Macromolecules,* 2009, **42**, 5642-5651.

55 A. Menelle, T. P. Russell, S. H. Anastasiadis, S. K. Satija and C. F. Majkrzak, *Phys. Rev. Lett.,* 1992, **68**, 67-70.

56 J. G. Kennemur, L. Yao, F. S. Bates and M. A. Hillmyer, *Macromolecules,* 2014, **47**, 1411-1418.

57 A. Nunns, J. Gwyther and I. Manners, *Polymer,* 2013, **54**, 1269-1284.

58 M. Ceresoli, F. F. Lupi, G. Seguini, K. Sparnacci, V. Gianotti, D. Antonioli, M. Laus, L. Boarino and M. Perego, *Nanotechnology,* 2014, **25**.

59 J. Y. Wang, J. M. Leiston-Belanger, J. D. Sievert and T. P. Russell, *Macromolecules,* 2006, **39**, 8487-8491.

60 J. Y. Wang, W. Chen, J. D. Sievert and T. P. Russell, *Langmuir,* 2008, **24**, 3545-3550.

61 H. Wu and Y. Cui, *Nano Today,* 2012, **7**, 414-429.

62 C. T. G. Knight, R. J. Balec and S. D. Kinrade, *Angew. Chem.-Int. Edit.,* 2012, **51**, 9900-9903.

Table 1 Molecular characteristics of the PS-b-PEO.

SAMPLE	$\bar{M}_{n\,(PS)}$ g/mol (SEC)	$I_{(PS)}$ (SEC)	$\bar{M}_{n\,(total)}$ g/mol (MO)	$\bar{M}_{w\,(total)}$ g/mol (SEC)	$I_{(tot)}$ (SEC)	$f_{(PS)}$ (SEC)	$f_{(PS)}$ (^{1}H-NMR)
PS-b-PEO	5500	1.05	10800	11550	1.07	0.51	0.52

Table 2: Vibration modes and peak positions in the FTIR spectra of the microphase separated BCP thin films for the addition of LiCl-THF and LiCl-ethanol after solvent annealing in toluene at 60^o C for 30 min.

Polymer block	Peak position (cm^{-1})	Vibration modes
PS	738	benzene bending
PS	1620, 1452	benzene ring stretching
PEO	825	$\rho(CH_2) + \delta(C\text{-}O\text{-}C)$, ρ = rock, δ = deformation mode
PEO	945	$\rho_s(CH_2) + \nu(C\text{-}C)$, ν = stretch, X_s = symmetric
PEO	960	$\rho_{as}(CH_2) + \nu(CH_2)$, X_{as} = assymmetric
PEO	1060	$\nu(C\text{-}C) + \rho(CH_2)$
PEO	1145, 1093, 1060	$\nu_s(C\text{-}O\text{-}C)$,
PEO	1241	$\tau_s(CH_2)$, τ = twist
PEO	1279	$\tau_{as}(CH_2)$,
PEO	1456	$\delta_s(CH_2)$,
PEO	1466	$\delta_{as}(CH_2)$
PEO	2881	$\nu_s(CH_2)$
PEO	2946	$\nu_{as}(CH_2)$
PEO	1245, 1295	C–O–C, bending mode

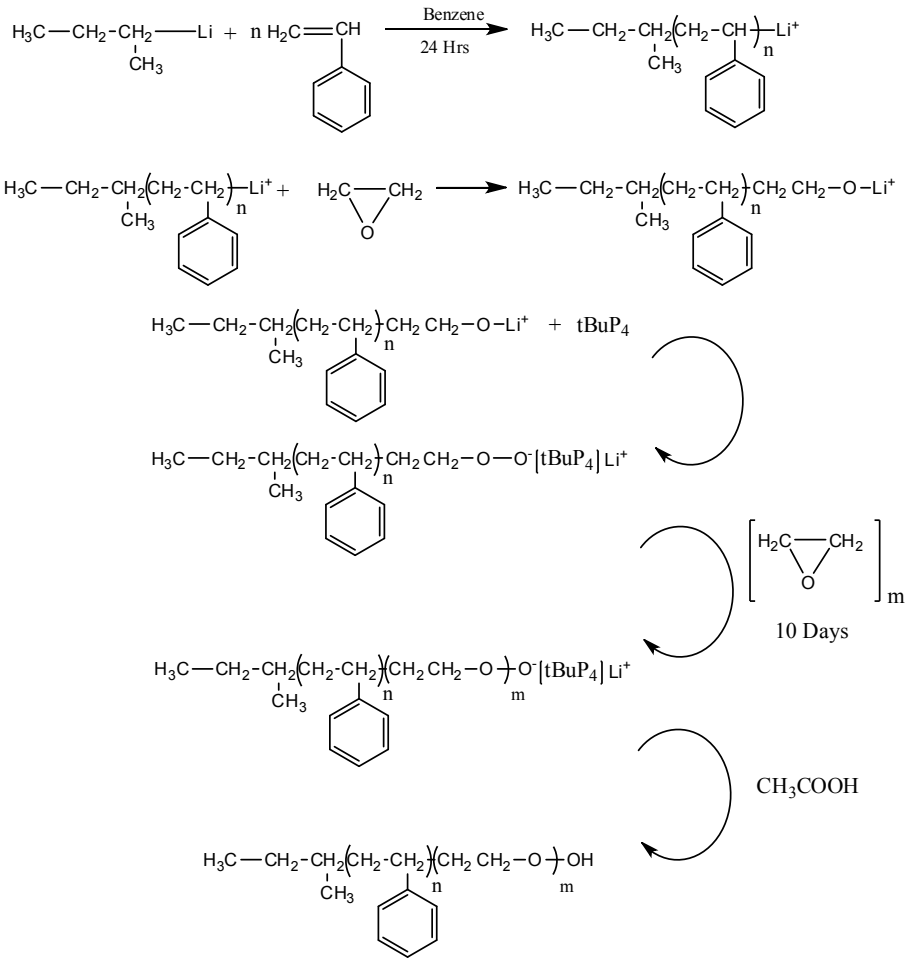

Scheme 1 Reactions for the synthesis of the lamellar PS-PEO diblock copolymer.

(a)

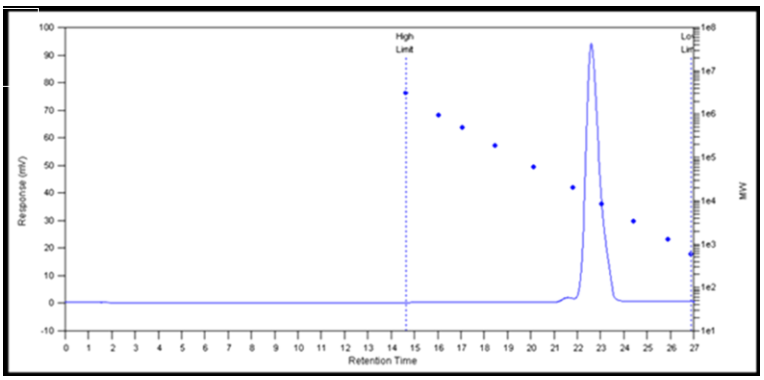

(b)

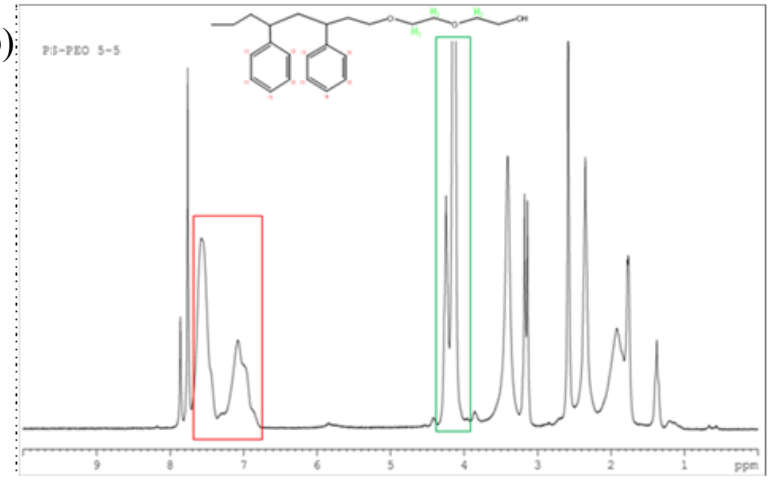

Scheme 2 (a) SEC chromatograph of the final diblock PS-b-PEO (b) ^{1}H-NMR spectra of sample PS-b-PEO indicating the chemical shifts of the four protons for PEO at ~4-4.5 ppm (green) and of the five aromatic protons for PS at ~6.8-7.5 ppm (red).

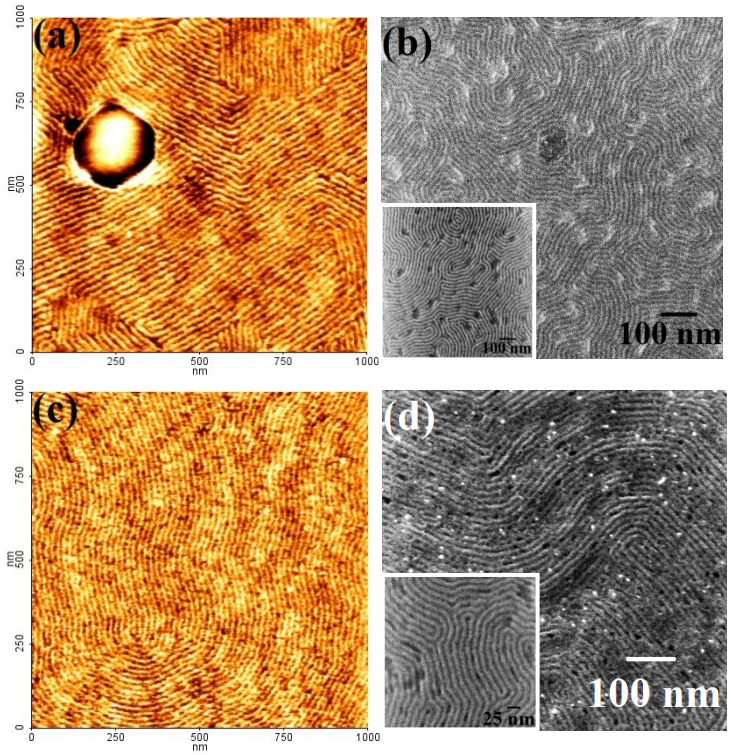

Fig. 1 (a, c) Tapping mode AFM images and (b, d) SEM images of the surface morphology of the PS-b-PEO thin film following solvent annealing in toluene at 60^{o} C for 30 min with the addition of 0.05 ml of (a, b) LiCl-ethanol and (c, d) LiCl-THF respectively.

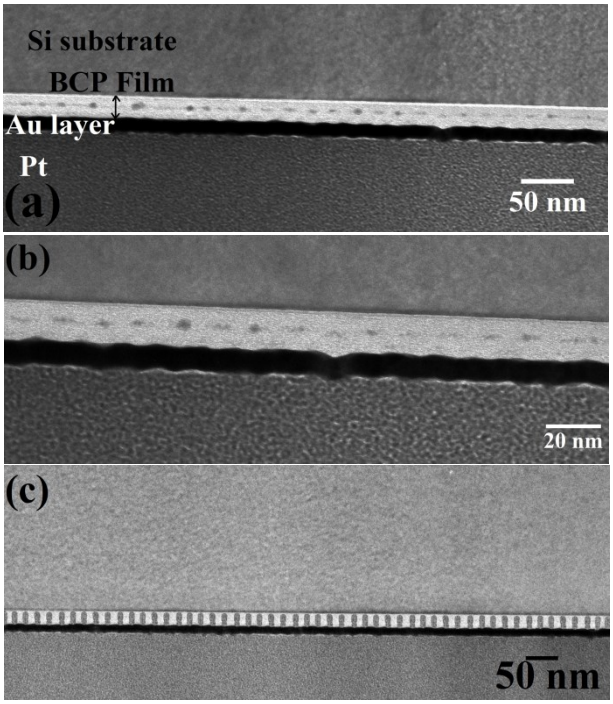

Fig 2 Cross-sectional TEM images of the periodic ordered lamellar film prepared with the addition of LiCl-THF after solvent annealing in toluene at 60^{o} C for 30 min (a) Large area view and (b) higher magnification image and (c) arrangement of lamellae after nickel precursor inclusion.

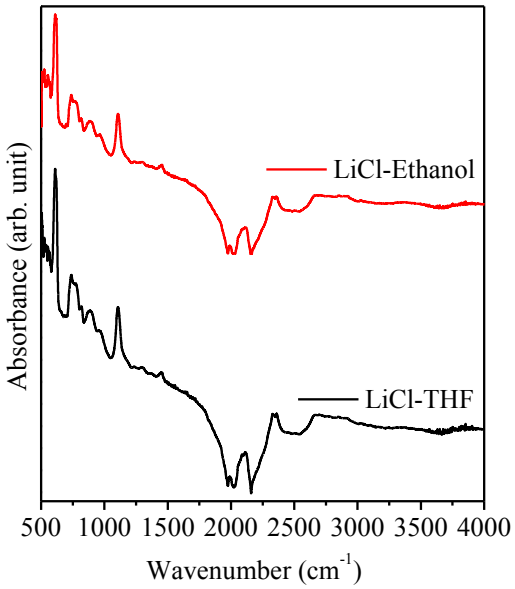

Fig 3 FTIR spectra of the BCP thin films for the addition of LiCl-THF and LiCl-ethanol after solvent annealing in toluene at 60^{o} C for 30 min.

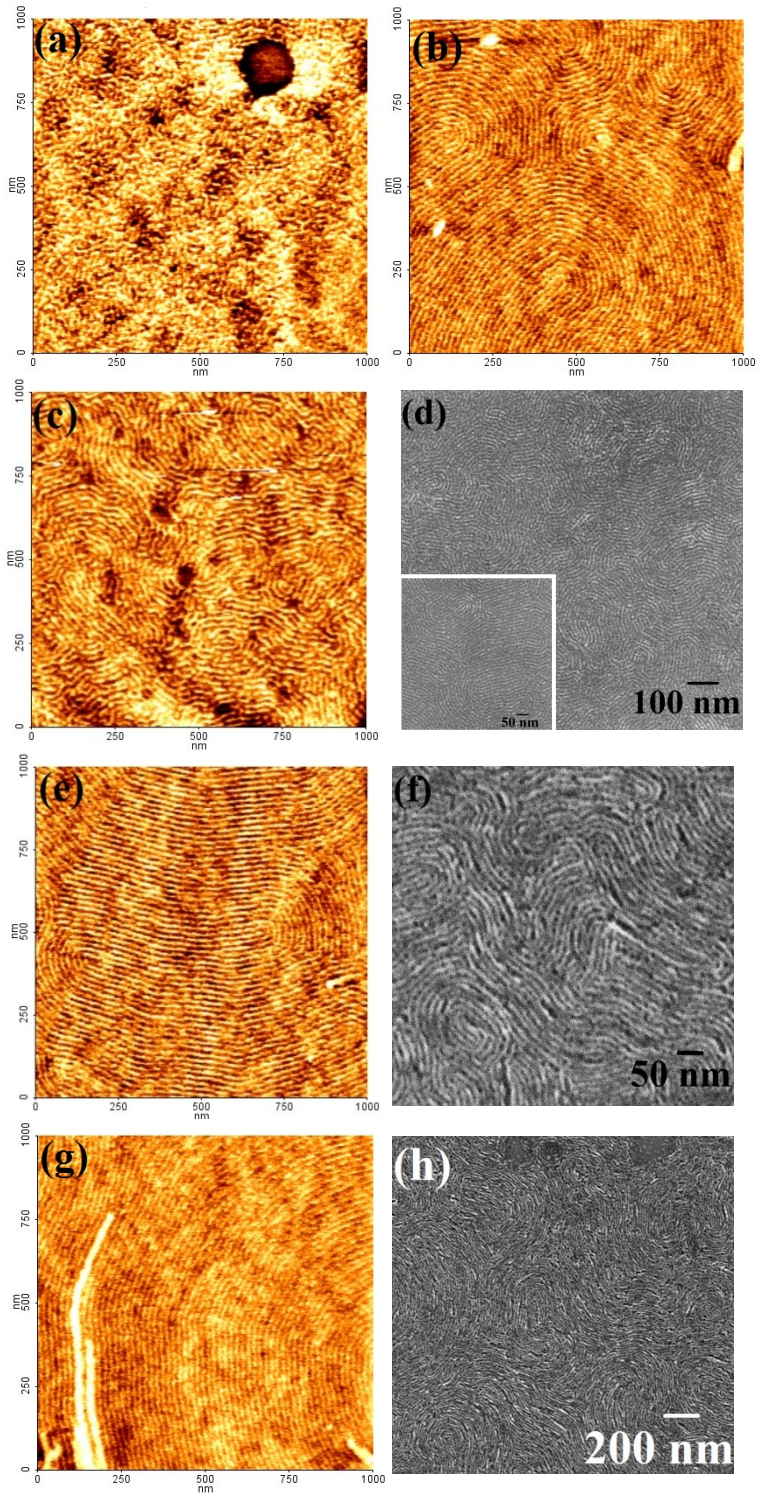

Fig 4 AFM images of the film annealed in toluene for 30 min at a temperature (a) 40^{o} C (b) 50^{o} C. (c, e, g) AFM and (d, f, h) SEM images of the film annealed in toluene at a temperature 60^{o} C for 15 min, 45 min and 1h respectively.

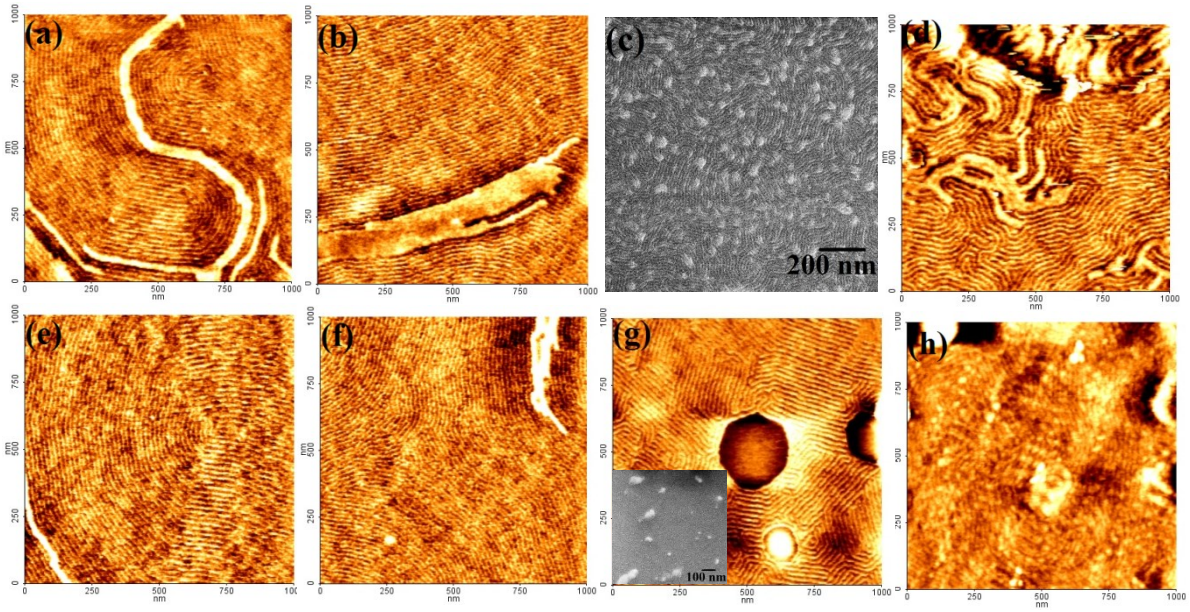

Fig 5 Surface morphology and topography of the films with LiCl-THF solution stirred for 30 min for the salt concentration of (a) 1 ml., (b, c) 1.25 ml., and (d) 1.5 ml. The variation in morphology of the films with 1 ml. of LiCl-THF solution for the stirring time of (e) 45 min, (f) 1h, (g, inset) 2h and (h) 3h.

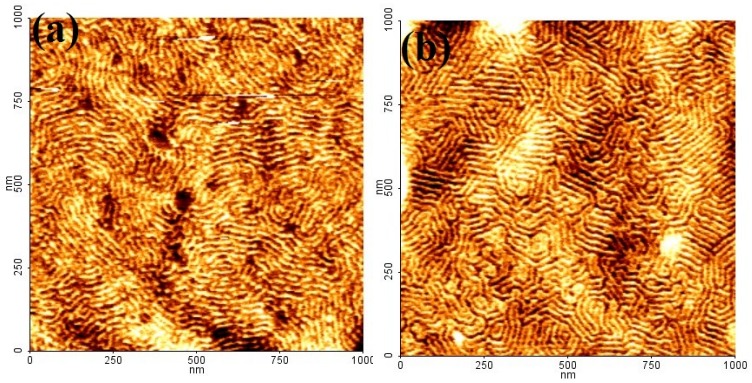

Fig 6 AFM images of the film with 1ml. of LiCl-THF solution solvent annealed in (a) THF and (b) Toluene/THF at 60^{o} C for 30 min.

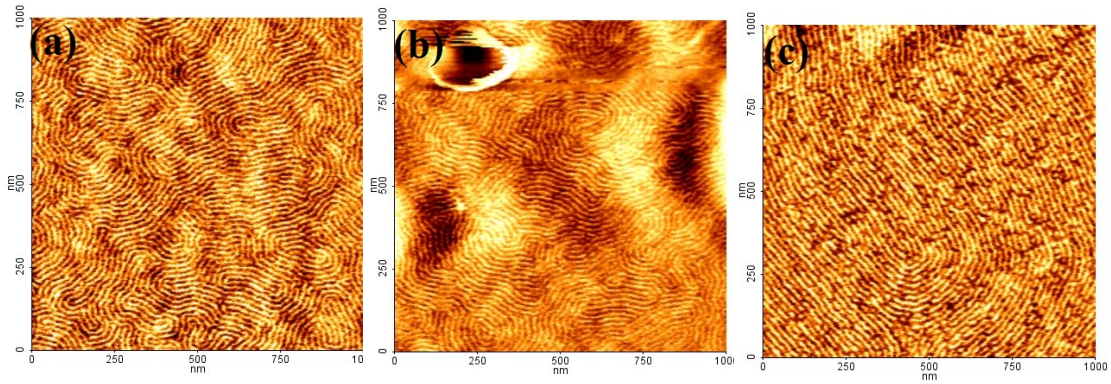

Fig. 7 Morphological evolution of the PS-b-PEO/LiCl system solvent annealed in toluene at 60^{o} C for 30 min on hard mask substrates (a) Si-ARC (anti-reflective coating), (b) alumina and (c) carbon hard mask (CHM).

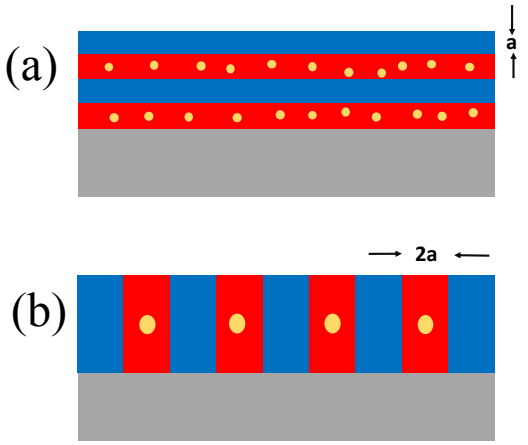

Scheme 3 Schematic illustration of the adjacent layers of PS and PEO (a) parallel and (b) perpendicular to the substrate surface after microphase separation with the co-ordination of the Li ions within the PEO block.